Optimised genome editing for precise DNA insertion and substitution using Prime Editors in zebrafish

Yosuke Ono[1], Martin Peterka[2], Michael Love[3], Amir Khan[4], Felix Bowers[4], Ashish Bhandari[1], Euan Gordon[2], Jonathan S. Ball[3], Chrissy L. Hammond[4], Charles R. Tyler[3], Steve Rees[5], Mohammad Bohlooly-Y[2], Marcello Maresca[2], and Steffen Scholpp[1*]

[1]Living Systems Institute, Biosciences, University of Exeter, United Kingdom; [2]Discovery Sciences, BioPharmaceuticals R&D, AstraZeneca, Gothenburg, Sweden; [3]Biosciences, University of Exeter, United Kingdom; [4]School of Physiology, Pharmacology; [5]Discovery Sciences, University of Bristol; [5]BioPharmaceuticals R&D, AstraZeneca, Cambridge, United Kingdom

*Correspondence: s.scholpp@exeter.ac.uk

Abstract

CRISPR/Cas9-mediated genome editing has rapidly become a popular tool for studying gene functions and generating genetically modified organisms. However, using this system, stochastic integration of random insertions and deletions restricts precise genome manipulation. Advanced CRISPR/Cas9 technologies using Prime Editors (PEs), Cas9 proteins fused with reverse transcriptase, enable programmed integration of short DNA modifications into the genome. However, its application in precise genome editing in animal models is challenging. Here, we utilise a nickase- and a nuclease-based PE to perform programmed short DNA substitution and insertion in various loci in the zebrafish genome. Whereas nickase-based PE2 mediated a higher ratio of precise prime edits to the total edits, nuclease-based PEn was more efficient for short DNA modifications, achieving up to 27.3% precise insertion. To further evaluate our approach, we inserted a nuclear localisation signal into a reporter transgene to incorporate longer fragments by prime editing. These gene modifications were transmitted to the next generation. We show that PE-mediated prime editing can efficiently manipulate genome information in zebrafish without using exogenous donor DNA.

Keywords Prime editing insertions

Prime editing, CRISPR/Cas9, zebrafish, PE2, PEn

Introduction

Genetically modified animals serve as powerful tools for studying ontogenesis and disease mechanisms in complex living systems. The zebrafish, *Danio rerio,* is a well-established model vertebrate species in cell and developmental biology due to attributes including its high fecundity in laboratory environments, transparency of the embryos, and amenability to the application of tools for transgenesis[1–3]. Zebrafish have also emerged as a powerful vertebrate model organism for studying human diseases, as they exhibit a substantial degree of genetic similarity with humans (around 70% of human genes having a corresponding gene in zebrafish)[4]. Several technologies for targeted mutagenesis, such as zinc finger nuclease (ZFN) and transcription activator-like effector nuclease (TALEN), have been employed in zebrafish to establish genetic loss-of-function mutants[5–8]. Most recently, CRISPR/Cas9-mediated genome editing has been introduced, significantly advancing target mutagenesis in nearly every model system, including zebrafish[9–13]. The CRISPR/Cas9 system has the potential to mimic disease phenotypes more accurately, allowing for the creation of identical genetic alterations corresponding to disease-causing mutations in humans. However, it has the disadvantage of stochastically generating insertions and deletions (so-called indels). This is because this technology relies on the DNA double-strand break (DSB) induced by the endonuclease at the target sequence in the genome and subsequent DNA repair. To allow precise control of genome editing, homology-directed repair (HDR)-mediated knock-in approaches using exogenous donor DNA have been utilised in zebrafish[14–16]. However, HDR-mediated precise genome editing occurs less efficiently compared with random mutagenesis.

Due to the need for precise genome editing with high efficiency, new strategies have been employed and applied in model organisms. For example, CRISPR/Cas9-mediated precise editing using Prime Editor has recently been developed, which does not rely on exogenous DNA donors. The original Prime Editor is a fusion protein of *Sp*Cas9 (H840A) nickase and Moloney murine leukaemia virus (MMLV) reverse transcriptase[17]. By combining the Prime Editor with a prime editing guide RNA (pegRNA), the resulting Prime Editor ribonucleoprotein (RNP) complex generates a single-strand break (SSB) or nick at the target site in the genome. The reverse transcriptase domain elongates an additional DNA sequence at the 3' end of cleaved DNA, following the reverse-transcription (RT) template sequence incorporated in the pegRNA. The additional short DNA fragment that contains the intended edit is integrated into the genomic DNA through the ligation of the 3' flap and the excision of the competing 5' flap from the original DNA sequence[17]. The Cas9-nickase-based Prime Editor enables programmed

short DNA modification (insertion, deletion and substitution), as has been shown in cultured cells, mouse and zebrafish embryos[17–20]. An alternative to the Cas9-nickase-based Prime Editor is prime editing with a Cas9-nuclease-based Prime Editor (PEn)[21–23]. PEn facilitates programmed short DNA modification through DNA repair based on homology annealing and non-homologous end joining (NHEJ) after DSB[22]. However, evidence for the successful use of Prime Editors in creating genetically modified animals is still limited. This is due to various technical challenges, including high variability in editing modes, low editing efficiency, and different delivery methods for prime editing components in living animals.

Here, we assess PE2, a nickase-based Prime Editor with additional mutations to optimise RT performance[17], and PEn-mediated prime editing for establishing genetically modified zebrafish for programmed DNA modification in their genome. We tested nucleotide substitution and the insertion of different lengths of DNA sequences. We performed morphological assessments of these genetically modified embryos. We show that PE2 mediates prime editing more accurately for short DNA insertion and base pair substitution in zebrafish embryos, whereas editing with PEn can more efficiently insert nucleotides up to 46 bp for modulating protein function and behaviour, all without using exogenous donor DNA. We further show that stable genetically modified zebrafish lines can be generated that inherit these programmed short DNA modifications.

Results

Prime editing in nucleotide substitution

First, we tested the use of Prime Editors for substituting specific base pairs in the zebrafish genome. To do this, we focused on the Cereblon (CRBN) gene, which has been associated with developing resistance to thalidomide-based treatments, particularly in conditions like multiple myeloma[24,25]. Here, we first compared the functioning of nickase-based PE2 and nuclease-based PEn, in which the H840A mutation is reverted to wild type[22], in nucleotide substitution in the zebrafish *crbn* gene (Fig. 1a), targeting the sequence encoding the amino acid residue I378 associated with the sensitivity to thalidomide and related drugs[26,27]. We designed a pegRNA to substitute 2 single nucleotides in the target sequence: one for introducing missense mutation in the I378 site (+10 A to G) and the other (+3 G to C) to prevent interaction between complementary sequences in the 5' spacer sequence and 3' primer binding site (PBS) and RT template sequence which potentially leads pegRNA misfolding[28,29] (Fig. 1b). A mixture of

100 Prime Editor proteins and chemically synthesised pegRNA was injected into zebrafish embryos
101 at the early 1-cell stage, after which the embryos were incubated at 32°C. Genomic DNA was
102 then extracted from these embryos at 96 hours post-fertilisation (hpf) to analyse genome edits
103 at the target site. Amplicon sequencing of the target region showed that both PEn and PE2
104 integrated the prime editing substitution into the genome (Fig. 1c). We found that PE2 had a
105 higher efficiency in precise substitutions (8.4%) compared to PEn (4.4%, Fig. 1d). Furthermore,
106 PEn induced a higher amount of indels (Fig. 1e). The precision score, defined as the ratio of
107 precise prime edits to the total edits, including imprecise prime edits and indels, was
108 significantly higher with PE2 (40.8%) compared to PEn (11.4%, Supplementary Fig. 1). We
109 also tested the refolding procedure of pegRNA by heat denaturation[28]. Refolding of the *crbn*
110 pegRNA did not enhance prime editing substitution with both PEn and PE2 (Fig. 1d). At the
111 *crbn* locus, PE2 is more effective for very short nucleotide substitutions compared with PEn in
112 zebrafish.

113

114 *Prime editing insertion of 3 bp DNA fragment*

115 Next, we tested the functioning of the Prime Editors in the precise insertion of a 3 bp stop
116 codon into the coding sequence of the endogenous target gene to generate a mutant allele that
117 produces a precisely truncated protein. As a proof-of-concept, we chose the cognate receptor
118 gene *ror2*. Genetic mutations in the *ROR2* gene in humans can cause the autosomal recessive
119 Robinow syndrome, leading to short stature, distinctive facial features, and skeletal
120 abnormalities, including short limbs and a curved spine (*scoliosis*)[30–33]. In zebrafish, the
121 inhibition of Ror2 signalling function affects the convergence and extension of axial cells
122 during gastrulation and the elongation of the embryo body, leading to a broader and shorter
123 body axis[34–37], as well as the patterning of cranial tissues[38], and thus would be an excellent
124 model for studying many aspects of the Robinow syndrome.

125 Sequence comparison suggested that the zebrafish W722X allele corresponds to the human
126 disease-related W720X mutation generating a premature stop codon (TGA) in the tyrosine
127 kinase domain (Fig. 2a). Therefore, we aimed to establish the zebrafish Robinow W722X
128 model by designing pegRNA and single primed insertion gRNA (springRNA)[22] generating a
129 similar stop codon into the sequence of exon 9 in zebrafish *ror2.* The pegRNA contained a 3
130 nt RT template sequence for the stop codon to be integrated, 13 nt PBS sequence, and 13 nt
131 sequence to extend the homology arm for the DNA integration via homology annealing (Fig.

132 2b and c). We compared this strategy to using a springRNA combined with PEn, without the
133 template sequence for the homology arm, to insert the stop codon via NHEJ (Fig. 2b and c).
134 We microinjected combinations of Prime Editor mRNA and guide RNA, that is, PE2/pegRNA,
135 PEn/pegRNA and PEn/springRNA at the one-cell stage in zebrafish embryos. The sequence in
136 *ror2* exon 9 was amplified by PCR from a pool of genomic DNA obtained from 10 injected
137 embryos, and the induction of DNA modification was assessed by a T7 endonuclease I (T7E1)
138 assay. We observed the cleavage of PCR products in the samples injected with PEn/pegRNA
139 and PEn/springRNA combinations, indicating sequence modification in the target site (Fig. 2d).
140 We were unable to detect obvious cleavage of heteroduplex DNA with PE2/pegRNA
141 combination, suggesting that PE2 induced fewer editing events compared to PEn.

142 The PCR products were also cloned into a cloning vector, and the target sequences in
143 randomly selected clones were analysed. Various types of edits in the target site were observed
144 in the clones from the PEn injected samples, including precise insertion of the stop codon
145 and/or random indels (Fig. 2e), although no sequence edits in the target site were identified
146 from the PE2 injected sample (0/44 clones; Supplementary Fig. 2). Subsequently, we
147 performed amplicon sequencing to quantify the proportion of each genome edit. We found that
148 the proportion of precise prime editing (only TGA insertion without any indels) was higher
149 when using PEn/pegRNA combination (10.3%) compared to PEn/springRNA (4.0%) and
150 PE2/pegRNA (0.4%, Fig. 2f). In addition, springRNA showed a higher proportion of imprecise
151 prime edit (TGA insertion with random indels; 37.5%) than pegRNA (11.1% and 0.2% with
152 PEn and PE2, respectively; Fig. 2f). The precision scores for the PE2/pegRNA, PEn/pegRNA,
153 and PEn/springRNA combinations were 58.9%, 32.6%, and 7.8%, respectively. This suggests
154 that prime editing via homology annealing with pegRNA was more accurate than via NHEJ
155 using springRNA.

156

157 *Comparison of the mode of Prime Editor delivery as mRNA or RNP complex*

158 Next, we compared PEn and PE2 in combination with different strategies of Prime Editor
159 delivery. Here, we performed amplicon sequencing with genomic DNAs extracted from
160 individual embryos injected with Prime Editor mRNA or RNP complex with the *ror2* pegRNA
161 (Fig. 3a). We found that the proportion of precise prime edit is significantly increased with PE2
162 RNP complex (11.5%) compared to PE2 mRNA (1.3%), whereas the there is no significant
163 difference between PEn RNP complex (20.5%) compared to PEn mRNA (18.8%; Fig. 3b).

However, with both delivery methods of the Prime Editors, the proportion of precise prime edit was significantly higher with PEn compared to PE2, supporting our previous results (Fig. 2f and 3b) although, PEn-mediated prime editing insertion outperformed HDR-mediated knock-in using single-stranded donor DNAs (2.3% and 5.2%; Fig. 3c). Furthermore, PEn also integrated a notably higher number of indels that are unrelated to prime editing (Fig. 3d), probably due to the DNA DSB induced by its nuclease activity as the indel frequency was similar level to the conventional HDR-mediated knock-in using Cas9 RNP complex (Supplementary Fig. 3a). These resulted in lower precision scores with PEn (34.3% and 28.2% for mRNA and RNP delivery, respectively) compared to PE2 (71.6% and 43.4% for mRNA and RNP delivery, respectively; Supplementary Fig. 3b). We also tested the generation of *ror2* W722X allele by single nucleotide substitution (TGG to TGA). Notably, PEn-mediated prime editing introduced targeted substitution (3.7%) more efficiently than PE2 (2.0%) in *ror2*, whereas PEn induced a higher amount of indels resulting in a lower precision score (14.8%) compared to PE2 (25.4%; Supplementary Fig. 3c–e). These findings suggest that the PEn-induced DNA DSBs are more likely to undergo repair events (both precise and imprecise) compared to the nickase-based PE2 method. Although PEn and PE2 showed distinct editing outcomes, both Prime Editors did not show a significant difference in the frequency of non-specific editing at 3 potential off-target sites in the genome, and their specificity was comparable to HDR-mediated knock-in using donor-DNA into the same target site (Supplementary Fig. 3f and g).

Inclusion of abasic spacer into springRNA to prevent guide RNA scaffold insertion

In the analysis of the sequence edits in the *ror2* gene by PEn-mediated prime editing, we found that a substantial proportion of the amplicons derived from embryos injected with the PEn/springRNA combination contained imprecise prime edits with additional nucleotides that correspond to the sequence of guide RNA scaffold adjacent to the RT template (Fig. 3e), as reported previously[18]. This finding suggests that the readthrough of RT from the template sequence into the guide RNA scaffold causes unintended insertions, as has also been reported in human cell lines[17,39]. Aiming to control the termination of RT in prime editing, we synthesised a modified springRNA in which an abasic RNA spacer was inserted between the RT template and guide RNA scaffold (Fig. 3f). Microinjection of the abasic springRNA together with PEn mRNA or RNP complex significantly reduced the unintended insertion of

196 guide RNA scaffold sequence into the target site (Fig. 3g). However, the proportion of precise
197 prime edits did not show a significant improvement (Fig. 3h). Due to the significantly reduced
198 number of the imprecise prime edits, the precision scores increased from 9.6% to 21.7% and
199 from 10.6% to 14.2% with PEn mRNA and RNP complex, respectively, through the blocking
200 of scaffold sequence incorporation (Supplementary Fig. 3h). These results suggest that the
201 read-through process is independent of precise genome editing events in zebrafish embryos,
202 unlike in human cultured cells[39].

203

204 *Prime editing in adgrf3b gene using PEn*

205 Next, we tested the PEn-mediated prime editing targeting at a different locus, here the
206 *adgrf3b* gene. A previously published study has reported that the efficiency of prime editing
207 in the *adgrf3b* gene using PE2 RNP complex was decreased from 18.0% to 0.1% by extending
208 the length of prime editing insertion from 3 bp to 12 bp[18]. Therefore, we compared the
209 efficiency of our nuclease-based PEn to PE2 by targeting the same sequence in the *adgrf3b*
210 gene to integrate the 3 bp or 12 bp insertion. Both PEn/pegRNA and PEn/springRNA
211 combinations successfully integrated the programmed 3 bp and 12 bp insertion into the target
212 site in the injected embryos. Here, the mean proportion of precise prime edit for 3 bp insertion
213 using PEn mRNA with pegRNA and springRNA was 27.3% and 4.0%, respectively, and 26.1%
214 and 2.9% using PEn RNP complex (Fig. 3i). For 12 bp insertion, the mean proportion of precise
215 prime edit using PEn mRNA with pegRNA and springRNA was and 1.9% and 0.7%,
216 respectively, and 8.3% and 0.9% using PEn RNP complex (Fig. 3j). The precision scores of
217 PEn mRNA with pegRNA and springRNA were 42.1% and 4.6% for a 3 bp insertion and 8.6%
218 and 1.1% for a 12 bp insertion, respectively (Supplementary Fig. 3i), suggesting that both the
219 efficiency and accuracy of prime editing declined with an increase in insertion length. Notably,
220 the PEn RNP complex with pegRNA performed more efficiently with the 12 bp insertion
221 compared to the PE2 system, this suggests that PEn-generated DNA DSB accepts longer
222 insertion than a nickase-based Prime Editor in zebrafish embryos. Inclusion of an RNA or DNA
223 spacer into the springRNAs did not improve prime editing insertion in *adgrf3b*, whereas the
224 incorporation of guide RNA scaffold was significantly reduced similarly to the *ror2* locus
225 (Supplementary Fig. 3j and k).

226

227 *Establishing stable ror2*^{W722X} *mutant zebrafish*

228 Having demonstrated the programmed insertion via PEn-mediated prime editing in injected
229 embryos, we wanted to establish if these precise edits are passed on to the next generation, as
230 this is a prerequisite for establishing a disease model. We, therefore, aimed to develop stable
231 *ror2*^{W722X} mutant zebrafish. Therefore, first, we injected embryos with PEn RNP complex and
232 the *ror2* springRNA and raised the embryos to adults, and then we outcrossed them with wild-
233 type fish to collect F1 embryos. Through genotyping 16 embryos from each F0 adult fish, we
234 obtained F1 embryos harbouring the *ror2*^{W722X} mutation. Six out of 10 F0 adults were founders
235 of the allele, with the rate of germline mosaicism varying between 6.3% (1/16) and 31.3%
236 (5/16; Fig. 4a). We raised the F1 heterozygous *ror2*^{W722X} fish and inbred them to generate
237 homozygous *ror2*^{W722X} mutant embryos in the F2 generation. The morphology of the zygotic
238 *ror2*^{W722X} mutant embryo and larvae was similar to wild-type siblings, and the mutant animals
239 were both viable and fertile (Fig. 4b, c and e). Subsequently, we generated maternal-zygotic
240 (MZ) mutants by in-crossing homozygous *ror2*^{W722X} male and female fish. The MZ *ror2*^{W722X}
241 mutant larvae at 5 dpf showed a mild curvature of the tail tip and shorter body length (Fig. 4d
242 and f), which are similar phenotypes to the MZ mutant larvae of the loss-of-function alleles in
243 *ror2* reported previously[34,38]. Zygotic and MZ mutant adults lacked craniofacial sensory organs,
244 nasal and maxillary barbels (Fig. 4g and h, and Supplementary Fig. 4), and 1 year old mutant
245 showed altered jaw morphology with a significantly altered aspect ratios in the mandible,
246 leading to a less protrusive lower jaw (Fig. 4i–m), phenocopying the larval and adult
247 phenotypes previously described for zebrafish *ror2* mutants[38]. These phenotypes also resemble
248 the craniofacial defects in *Ror2* mutant mice[40] and the micrognathia observed in human patients
249 with Robinow syndrome[32,33]. This suggests that the human disease-related *ror2*^{W722X} mutation
250 in the tyrosine kinase domain affected the Wnt/PCP signalling similarly to the observation in
251 patients with Robinow syndrome. This set of data suggests that PEn-based editing can be used
252 to establish stable genetically modified fish lines for disease modelling.

253

254 *Insertion of nuclear localisation signal into transgenic reporter gene*

255 After the successful insertion of the 3 bp stop codon into the *ror2* gene to establish a
256 zebrafish model of the Robinow syndrome and successful 3 and 12 bp insertions into the
257 *adgrf3b* gene, we tested whether PEn-mediated prime editing can be used to integrate longer
258 insertions. Since we anticipated that these events would be rare, we employed a strategy that
259 enabled us to screen for prime edit events and distinguish between imprecise prime edits and

260 random indels at the cellular level in living zebrafish embryos, all without the need for time-
261 consuming sorting and genetic analysis. This was achieved using an eGFP-transgenic fish line
262 with an introduced nuclear localisation sequence (NLS) of 27 bp using PEn. We anticipated
263 three phenotypes: cytosolic GFP localisation for unsuccessful editing, no GFP expression for
264 imprecise edits, and nuclear GFP expression for precise prime editing insertion (Fig. 5a). We
265 subsequently mapped these effects in individual cells using high-resolution confocal
266 microscopy in living zebrafish larvae. Specifically, we tested the insertion of the NLS sequence
267 into the *smyhc1:gfp* transgene by prime editing. The *smyhc1:gfp* reporter gene is expressed
268 explicitly in the superficial slow-twitch muscle fibres in the body trunk (Supplementary Fig.
269 5a), which are mononuclear during embryonic development[41]. We designed pegRNAs that
270 target the N-terminal end of the eGFP coding sequence in the *smyhc1:gfp*^{i104} transgenic allele
271 and contain RT template sequence for inserting c-myc NLS[42–44]. We expected that precise
272 integration of the 30 bp sequence, including 27 bp c-myc NLS and 3 bp spacer, translocates
273 the eGFP expression from the cytoplasm to the nucleus in the muscle fibres, whereas reporter
274 expression is lost in the cells with imprecise prime edits or random indels by frameshifting in
275 the eGFP coding sequence (Fig. 5a). The embryos injected with PEn RNP complex showed
276 mosaic expression of eGFP in the cytoplasm of muscle fibres, lack of GFP expression in some
277 fibres along with the accumulation of eGFP signals in a few cell nuclei (Fig. 5b). Amplicon
278 sequencing of the target region in the genome showed that the average efficiency of precise
279 prime editing insertion in the whole injected embryo was 8.5% with a precision score of 9.7%
280 (Fig. 5c). We also compared the prime editing efficiency to that using a longer pegRNA in
281 which PBS sequence and template sequence of the homology arms were extended from 10 nt
282 to 13 nt and 14 nt to 36 nt, respectively. However, the prime editing efficiency of the longer
283 pegRNA was significantly decreased, possibly due to increased RNA complexity leading to
284 altered secondary structures (Fig. 5c).

285 Next, to establish stable genetically modified zebrafish lines with the NLS insertion, we
286 raised F0 injected fish to adults, outcrossed them with wild type, and screened the F1 embryos
287 for their GFP expression. Although 8.0% (7/87) of injected F0 fish showed mosaic eGFP
288 expression with nuclear eGFP at 3 dpf, there was a difficulty in estimating prime editing
289 efficiency by the observation, as muscle fibres showed variable ratios of nuclear eGFP to
290 cytoplasmic eGFP; therefore, we did not pre-screen them for raising. We successfully isolated
291 embryos showing pronounced eGFP expression in the nuclei of slow-twitch fibres (Fig. 5d and
292 Supplementary Fig. 5b). We confirmed the integration of the 30 bp sequence into the eGFP

293 coding sequence (Fig. 5e and Supplementary Fig. 5c). Notably, multiple types of edits were
294 also identified in the amplicons obtained from the single embryo with nuclear eGFP expression,
295 suggesting that the *smyhc1:gfp*^{i104} transgenic allele contains at least 4 copies in this locus. Each
296 copy was targeted and edited individually by PEn/pegRNA complex (Fig. 5e and
297 Supplementary Fig. 5c). Here, 4 F0 adult fish out of 6 screened were identified as founder fish
298 of the prime editing insertion in the target transgene. The proportion of the embryos showing
299 nuclear eGFP expression varied between 1.4 to 20.2% (Fig. 5f).

300 To challenge the length of insertion using PEn in zebrafish embryos further, we also tested
301 the insertion of a 46 bp attP sequence for attP/attB recombination by phiC31 integrase, which
302 could expand the application of PEn for transgenesis[45–47]. Microinjection of PEn RNP complex
303 with springRNA that contains RT template for inserting a 46 bp attP sequence into *wls* gene
304 achieved the programmed insertion at the efficiency of 1.4% with a precision score of 2.9%,
305 and the efficiency was comparable to HDR-mediated knock-in into the same target site using
306 single-stranded donor DNAs (1.4% and 0.5%; Supplementary Fig. 6). Our findings indicate
307 that PEn-mediated precise DNA insertion is a practical tool for the accurate integration of
308 functional motifs with a length of up to 46 bp within a target gene in zebrafish.

309

310 **Discussion**

311 *The need for precise genome editing*

312 Target sequence-specific mutagenesis and transgenesis are essential tools for analysing gene
313 functions, and labelling expressed proteins, cellular components and specific cell types *in vivo*.
314 Induction of DSB in the genome DNA by ZFN, TALEN and CRISPR/Cas9 technologies
315 enable random mutagenesis and donor DNA-based knock-in in the target sequence. In addition
316 to the conventional HDR-mediated knock-in, multiple systems for targeted integration into the
317 genome in zebrafish have been reported[47,48]. Adding further to this, Cas9-nickase fusion
318 proteins with cytidine or adenine deaminase, so-called Base Editors[49,50], enable single
319 nucleotide substitution in zebrafish to generate human disease models[51–56]. Despite
320 advancements in gene editing technologies, however, the application of Prime Editors for the
321 generation of genetically modified animals remains restricted[18,57–59]. This limitation can be
322 attributed to several technical hurdles, including substantial variability in editing modes,
323 suboptimal editing efficiency, and complications associated with the delivery of prime editing
324 components *in vivo*.

325 In this study, we established programmed short DNA modification in the genome using
326 Prime Editors and generated stable genetically modified zebrafish lines with 3 and 30 bp
327 insertions. Firstly, we utilised PE2 for successful nucleotide substitution in a target sequence
328 associated with drug sensitivity and PEn to generate a zebrafish model for human genetic
329 disease. Specifically, we established a stable *ror2*^{W722X} mutant line, which genocopies the
330 disease-related W720X mutation in the human *ROR2* gene. Various mutations have been
331 identified in the human *ROR2* gene as the causes of Robinow syndrome, and different types of
332 mutation lead to distinct phenotypes and inheritance patterns, possibly due to nonsense-
333 mediated decay of mutated mRNA[60], the mechanism which is also essential for embryonic
334 development and tissue homeostasis in zebrafish[61,62]. Our establishment of the *ror2*^{W722X} line
335 supports the use of prime editing to generate zebrafish models of disease-relevant alleles in
336 cases where short, programmed substitutions or insertions are sufficient. Using prime editing
337 and base editing by Base Editors will open a wider window for precise genome editing in
338 zebrafish for both drug discovery and human disease models.

339 Secondly, we inserted a functional motif in existing lines to control the features of a protein.
340 Here, specifically, we inserted an NLS sequence into the *smyhc1:gfp*^{i104} transgene and assessed
341 the prime editing *in vivo* by translocating eGFP expression. The same approach can be applied
342 to tag endogenous proteins and control their localisation and transport. The pegRNAs we used
343 to insert NLS were designed in the coding sequence of the N-terminal region of eGFP, and
344 therefore, the strategy can be used for other established eGFP reporter zebrafish lines to convert
345 their GFP expression from the cytoplasm to the cell nuclei and as a control to assess prime
346 editing *in vivo* morphologically.

347 Previous studies have reported a low efficiency of prime editing insertion. In those studies
348 it is proposed that the length negatively correlates with prime editing efficiency, while the
349 MLH1 protein influences editing outcomes for short sequences up to 13 bp in cultured cells[63–
350 65]. Indeed, we observed the declined efficiency and accuracy of prime editing with extended
351 insertion in zebrafish embryos. However, the insertion of the 30 bp NLS into the *smyhc1:gfp*
352 transgene showed similar or higher editing efficiency to the 12 bp insertion into the *adgrf3b*
353 gene, suggesting that other factors such as spacer sequence and/or complexity of pegRNA also
354 affect the prime editing efficiency[63]. Enhancing pegRNA stability and preventing degradation
355 can further improve editing efficiency[28,29,66]. Finally, co-expressing effector proteins with
356 Prime Editor to suppress undesired DNA repair pathways or protect pegRNA from degradation
357 has been suggested to enhance editing[23,64,67]. Evaluation of these technologies in zebrafish[68,69],

358 as well as codon optimisation of Prime Editors and adaptation to RT at lower temperature, will
359 advance precise genome manipulation *in vivo* further.

360

361 *The underlying mechanism of PEn-mediated precise genome editing*

362 Here, we demonstrated that a nuclease-based PE can efficiently integrate DNA insertions
363 between 3–46 bp in zebrafish embryos. By utilising pegRNA and springRNA, we show that
364 the integration is based on both homology annealing and NHEJ, as suggested in cell culture[22].
365 Although pegRNA performed better under the tested conditions than springRNA in both
366 efficiency and accuracy at the tested target loci, springRNA could be advantageous when
367 longer PBS and/or RT template sequences are necessary, as it lacks a template for homology
368 arms. We also observe that the repair outcome varies depending on the delivery mode of the
369 PEn. Microinjection of PEn mRNA leads to fewer indels than supplying the PEn as an RNP
370 complex, although there was no significant difference in the level of precise prime edit in the
371 3 bp insertion at *ror2* and *adgrf3b* loci (Fig. 3). We hypothesise that the RNP complex acts
372 faster than the mRNA and a potential explanation could be that the relatively rapid integration
373 of random indels is more effective than the prime editing reaction in the early zebrafish embryo
374 (0–3 hpf), when cell cycle time is significantly shorter (approximately 25 min). However, the
375 precise DNA repair mechanism and accessibility to a target site in the genome for the prime
376 editing reaction in relation to the cell cycle duration need to be explored in the future.

377 We also show that nuclease-based PE has its limitations. For example, we found that the
378 nickase-based PE2 showed higher precision scores in nucleotide substitution and short DNA
379 insertion, as shown for *crbn* (Fig. 1 and Supplementary Fig. 1) and *ror2* (Supplementary Fig.
380 3). Further analyses will be required to compare nuclease-based and nickase-based Prime
381 Editors, focusing on the distance between the substitution sites and Cas9 nicking/cleavage site.
382 Furthermore, as PEn functions via DSB of genomic DNA, insertion can potentially cause off-
383 target effects, large deletions, and chromosomal rearrangements[70–72], whereas the level of large
384 deletions in PEn-mediated prime editing is comparable to that with the nickase-based PE2 in
385 cultured cells[22]. It will be interesting to see whether these adverse effects that occurred in
386 injected zebrafish can be neutralised by outcrossing against wild-type fish in the next
387 generations.

388 In conclusion, we have established genetically modified zebrafish with programmed short
389 DNA modifications by microinjecting Prime Editor mRNA or RNP complex with gRNAs that

integrate DNA modification via different DNA repairing pathways. PEn-mediated prime editing insertions were germline-transmitted to the next generation in the tested loci with measurable efficiency to establish stable genetically modified zebrafish lines. Our data establish prime editing-mediated insertion in zebrafish embryos as a practical donor DNA-free approach for precise short DNA modification, although editing efficiency and precision remain locus- and edit-dependent. The method can be employed to manipulate coding sequences in endogenous genes and to insert functional DNA motifs for protein tagging and modulating gene expression. Our data support the utility of PE2 for accuracy and PEn for efficiency in short DNA modifications in F0 injected zebrafish, while broader comparison of germline transmission efficiencies between prime editing systems will require future work.

400 **Materials and Methods**

401 *Zebrafish strains and husbandry*

402 Wild-type zebrafish strains WIK and AB and the *Tg(smyhc1:gfp)*^{i104} transgenic line[41] were
403 used to provide embryos. The collected embryos were raised at 28°C. Adult fish stocks were
404 reared and maintained in the Aquatic Resources Centre at the University of Exeter under the
405 conditions stated in the previous study[73]. The experimental procedures involving the animals
406 were reviewed and approved by the United Kingdom Home Office under the Animals
407 Scientific Procedures Act 1986 (project license: PP3975835) and received ethical approval
408 from the Animal Welfare and Ethical Review Body at the University of Exeter.

409

410 *Preparation of pegRNA and springRNA*

411 The sequences of the pegRNA and springRNA for prime editing in the *crbn*, *ror2*, and *wls*
412 genes, and for the *smyhc1:gfp* transgene, are listed in Supplementary Table 1. The pegRNAs
413 for prime editing insertion in the *adgrf3b* gene have been reported in a previous study[18]. The
414 first three nucleotides and inter-nucleotide linkages at both ends of the gRNA were chemically
415 modified with 2'-O-methylation and phosphorothioate, respectively. Chemically modified
416 synthetic gRNAs were obtained from Integrated DNA Technologies. The springRNAs with an
417 RNA or DNA spacer were sourced from Horizon Discovery and GenScript Biotech.
418 Synthesised gRNAs were dissolved in nuclease-free duplex buffer (Integrated DNA
419 Technologies) at 100 µM and stored at −20°C.

420

421 *Microinjection*

422 Microinjection into one-cell stage embryos was carried out under a stereomicroscope using a
423 FemtoJet 4x microinjector (Eppendorf). To prepare an injection mixture for prime editing, 1.25
424 µl of 600 ng/µl Prime Editor mRNA or 0.6 µl of 10 mg/ml purified Prime Editor protein was
425 combined with 2.5 µl of 12 µM gRNA and 0.5 µl of 0.5% phenol red (Sigma), and the volume
426 was adjusted to 5 µl with 2 M potassium chloride. PEn and PE2 mRNA were synthesised from
427 the linearised plasmids[22] using the mMESSAGE mMACHINE T7 kit (Invitrogen), following
428 the manufacturer's instructions. Purified Prime Editor proteins were prepared according to the
429 protocol in the previous study[39]. For HDR-mediated knock-in, 1.25 µl of 20 µM EnGen Spy

430 Cas9 NLS protein (New England Biolabs) was combined with 2.0 µl of 12 µM gRNA, 0.5 µl
431 of 500 ng/µl Alt-R single-stranded donor DNA, and 0.5 µl of 0.5% phenol red, and the volume
432 was adjusted to 5 µl with 2 M potassium chloride. Chemically modified single-stranded donor
433 DNAs were obtained from Integrated DNA Technologies. A mixture of Prime Editor or Cas9
434 protein and gRNA was incubated at 37°C for 5 minutes prior to microinjection to form an RNP
435 complex. Glass needles for microinjection were prepared from glass capillaries (TW100F-4,
436 World Precision Instruments) using a P-1000 micropipette puller (Sutter Instrument).
437 Approximately 1–1.7 nl of the injection mixture was injected per embryo. After microinjection,
438 the injected embryos were incubated in E3 embryo medium (5 mM sodium chloride, 0.17 mM
439 potassium chloride, 0.33 mM calcium chloride, and 0.4 mM magnesium chloride; pH 7.2) at
440 32°C, following the protocol by Petri et al[18].

441

442 *DNA extraction, PCR analyses and molecular cloning*

443 Genomic DNA was extracted from individual embryos and larvae using the modified
444 HotSHOT method[74]. The target region for prime editing in *ror2*, *adgrf3b*, and *smyhc1:gfp* was
445 amplified by PCR using the following primer sets: *ror2* (5'-AAACTTATGGGTGCCAGTCC-
446 3' and 5'-ATGGACACAAACTGAGGCTG-3'), *adgrf3b* (5'-
447 TGATTGCATACACACCTGACC-3' and 5'-AGGCACCTGCAGGAAAATTA-3'), and
448 *smyhc1:gfp* (5'-TGCAGTTACAAGGTACAGAGGTC-3' and 5'-
449 CGTCCTTGAAGAAGATGGTGCG-3'). The PCR mixture was prepared as follows: 10 µl of
450 2x PCRBIO Taq Mix red (PCR Biosystems), 0.8 µl each of 10 µM forward and reverse primers,
451 1 µl of genomic DNA pooled from 10 individual samples, and 7.4 µl of water, totalling a
452 volume of 20 µl. The PCR settings were as follows: 95°C for 1 min; 28 cycles of 95°C for 15
453 s, 58°C for 15 s, and 72°C for 15 s, followed by 72°C for 1 min. The mutation in the target
454 sequence of the PCR product was assessed by the T7 endonuclease I (T7E1) assay. PCR
455 products were denatured at 95°C for 5 min and then cooled to room temperature to form
456 heteroduplex DNAs. Subsequently, 5 µl of PCR product was mixed with 1 µl of NEBuffer 2
457 (New England Biolabs), 0.15 µl of T7E1 enzyme (10 U/µl, New England Biolabs), and 3.85
458 µl of water to a total volume of 10 µl and incubated at 37°C for 15 min. The PCR and T7E1-
459 digested products were assessed on a 3% agarose gel alongside a 100 bp DNA ladder (New
460 England Biolabs). PCR products were also cloned into the pGEM-T Easy vector (Promega)
461 and used for transformation with One Shot TOP10 chemically competent cells (Invitrogen)

following the manufacturer's instructions. Bacterial colonies grown on an LB agar plate with 100 µg/ml ampicillin were randomly selected and used for plasmid extraction using a GeneJET plasmid miniprep kit (Thermo Scientific). Sanger sequencing of PCR products and plasmids was performed by Eurofins Genomics.

Amplicon sequencing and bioinformatics

PCR amplicons for next-generation sequencing (NGS) of *adgrf3b*, *crbn*, *ror2*, *wls*, and *smyhc1:gfp* were prepared using Phusion Flash High-Fidelity 2x Mastermix (F548, Thermo Scientific) in a reaction volume of 15 µl, which contained 1.5 µl of genomic DNA extract and 0.2 µM of specific primers with barcodes and adapters for NGS. All primer sequences are shown in Supplementary Table 2. The PCR protocol with Phusion Flash High-Fidelity 2x Mastermix included an initial step at 98°C for 3 min, followed by 30 cycles at 98°C for 10 s, 60°C for 5 s, and 72°C for 5 s. The resulting PCR amplicons were purified using the HighPrep PCR Clean-up System (MagBio Genomics). The characterisations of size, purity, and concentration of the amplicons were conducted using a fragment analyser (Agilent). A second PCR was carried out to add Illumina indexes to the amplicons, utilising KAPA HiFi HotStart Ready Mix (Roche) in a total volume of 25 µl, containing 0.067 ng of PCR template and 0.5 µM indexed primers (Illumina). The PCR conditions were set at 72°C for 3 min, 98°C for 30 s, followed by 10 cycles at 98°C for 10 s, 63°C for 30 s, and 72°C for 3 min, with a 5-minute final extension at 72°C. Amplicons were purified with the HighPrep PCR Clean-up System (MagBio Genomics) and analysed using a fragment analyser (Agilent). Quantification was performed using a Qubit 4 Fluorometer (Life Technologies), with sequencing carried out on the Illumina NextSeq system in accordance with the manufacturer's guidelines. Demultiplexing of the amplicon sequencing data was executed with bcl2fastq software. The resulting fastq files were processed with CRISPResso2 V2.2.12 in prime editing mode[75]. Detailed parameters of the CRISPResso analysis can be found in Supplementary Table 3.

Live imaging

Stereomicroscope images were obtained using an Olympus DP73 microscope camera, and measurements were conducted with cellSens imaging software (Olympus). Confocal images of *smyhc1:gfp* transgene expression were captured with a Leica TCS SP8 laser scanning

microscope using a HC Fluotar L 25×/0.95 water objective and LAS X imaging software (Leica). For imaging, live zebrafish larvae were affixed to glass slides with 1% low melting agarose (5806A, Takara) in an E3 embryo medium containing 200 µg/ml tricaine (A5040, Sigma).

Computed Tomography

Adult wild-type and *ror2*^{W722X} mutant zebrafish at 12 months were fixed in 4% PFA for one week and dehydrated in 70% ethanol. Full body scans were taken using a Nikon XT H 225ST CT scanner (X-ray source of 130 kV and 53 µA without additional filters) with a voxel size of 20 µm. The generated scans were reconstructed using CT Pro 3D software (Nikon). During reconstruction, greyscale values were calibrated against a scan of a phantom with known density (0.75 g/cm^3). To evaluate shape changes while controlling for isometric growth, ratios of linear distances between annotated geographical points in three-dimensionally segmented reconstructions were calculated. Image renders and morphological analyses were performed using volume rendering function of Avizo software (FEI).

Statistics

Data visualisation and statistical analyses were conducted using GraphPad Prism 10.4 (GraphPad Software), BioRender Graph (R version 4.2.2), and Adobe Illustrator. For statistical analysis, the numerical dataset from each experimental condition was examined using the Shapiro-Wilk test for normality and Levene's test for homogeneity of variance. One-way ANOVA with Tukey multiple comparison test was utilised to assess differences between three or more groups with similar standard deviations, and Welch's one-way ANOVA with Dunnett T3 multiple comparison test for the groups having unequal variances (parametric). The Kruskal-Wallis test with Dunn's multiple comparison test was utilised to assess differences between the groups that are not normally distributed (nonparametric). Unpaired t-test (parametric) and the Mann-Whitney U test (nonparametric) were employed to evaluate differences between the two groups. The sample size for each experiment is presented in the figures and legends.

Acknowledgements

Research in the S.S. lab, including Y.O. and A.B., is supported by the Biotechnology and Biological Sciences Research Council Industrial Partnership Awards with AstraZeneca (BBSRC-IPA, BB/X008401/1; awarded to S.S., Y.O., and C.R.T) and the Living Systems Institute Open Innovation Platform Fund at the University of Exeter (awarded to Y.O.). M.L. receives support from the National Centre for the Replacement, Refinement and Reduction of Animals in Research (NC3Rs) PhD studentship (NC/X001407/1; awarded to J.S.B and C.R.T). C.L.H acknowledges funding from Versus Arthritis Senior fellowship (29317). A.K. was funded by GW4 BioMed MRC Doctoral Training Partnership, and F.B. by the South West Biosciences Doctoral Training Partnership (SWBio-DTP). We thank the Aquatic Resources Centre at the University of Exeter for the care of zebrafish resources.

Author contributions

Y.O., M.P., M.M., and S.S. conceived the study and designed the experimental strategy. Y.O., M.L., and A.B. performed the animal experiments and Y.O. and M.P. analysed the data with support from E.G., J.S.B., C.R.T., S.R., and M.B. Computed Tomography and the image analysis were conducted by A.K., F.B., and C.L.H. The manuscript was prepared by Y.O. and S.S.

Competing interests

M.P., E.G., S.R., M.B., and M.M. are employees of AstraZeneca and may be AstraZeneca shareholders.

References

1. Kwan, K. M. et al. The Tol2kit: a multisite gateway-based construction kit for Tol2 transposon transgenesis constructs. *Dev. Dyn.* **236**, 3088–3099 (2007). 10.1002/dvdy.21343.

2. Grabher, C., Joly, J. S. & Wittbrodt, J. Highly efficient zebrafish transgenesis mediated by the meganuclease I-SceI. *Methods Cell Biol.* **77**, 381–401 (2004). 10.1016/s0091-679x(04)77021-1.

3. Thermes, V. et al. I-SceI meganuclease mediates highly efficient transgenesis in fish. *Mech. Dev.* **118**, 91–98 (2002). 10.1016/s0925-4773(02)00218-6.

4. Patton, E. E., Zon, L. I. & Langenau, D. M. Zebrafish disease models in drug discovery: from preclinical modelling to clinical trials. *Nat. Rev. Drug Discov.* **20**, 611–628 (2021). 10.1038/s41573-021-00210-8.

5. Meng, X., Noyes, M. B., Zhu, L. J., Lawson, N. D. & Wolfe, S. A. Targeted gene inactivation in zebrafish using engineered zinc-finger nucleases. *Nat. Biotechnol.* **26**, 695–701 (2008). 10.1038/nbt1398.

6. Doyon, Y. et al. Heritable targeted gene disruption in zebrafish using designed zinc-finger nucleases. *Nat. Biotechnol.* **26**, 702–708 (2008). 10.1038/nbt1409.

7. Huang, P. et al. Heritable gene targeting in zebrafish using customized TALENs. *Nat. Biotechnol.* **29**, 699–700 (2011). 10.1038/nbt.1939.

8. Sander, J. D. et al. Targeted gene disruption in somatic zebrafish cells using engineered TALENs. *Nat. Biotechnol.* **29**, 697–698 (2011). 10.1038/nbt.1934.

9. Varshney, G. K. et al. High-throughput gene targeting and phenotyping in zebrafish using CRISPR/Cas9. *Genome Res.* **25**, 1030–1042 (2015). 10.1101/gr.186379.114.

10. Jao, L. E., Wente, S. R. & Chen, W. Efficient multiplex biallelic zebrafish genome editing using a CRISPR nuclease system. *Proc. Natl. Acad. Sci. USA.* **110**, 13904–13909 (2013). 10.1073/pnas.1308335110.

11. Hwang, W. Y. et al. Efficient genome editing in zebrafish using a CRISPR-Cas system. *Nat. Biotechnol.* **31**, 227–229 (2013). 10.1038/nbt.2501.

12. Burger, A. et al. Maximizing mutagenesis with solubilized CRISPR-Cas9 ribonucleoprotein complexes. *Development* **143**, 2025–2037 (2016). 10.1242/dev.134809.

13. Wu, R. S. et al. A rapid method for directed gene knockout for screening in G0 zebrafish. *Dev. Cell* **46**, 112–125 (2018). 10.1016/j.devcel.2018.06.003.

14. Hoshijima, K., Jurynec, M. J. & Grunwald, D. J. Precise editing of the zebrafish genome made simple and efficient. *Dev. Cell* **36**, 654–667 (2016). 10.1016/j.devcel.2016.02.015.

15. DiNapoli, S. E. et al. Synthetic CRISPR/Cas9 reagents facilitate genome editing and homology directed repair. *Nucleic Acids Res.* **48**, e38 (2020). 10.1093/nar/gkaa085.

580 16. Levic, D. S., Yamaguchi, N., Wang, S., Knaut, H. & Bagnat, M. Knock-in tagging in
581 zebrafish facilitated by insertion into non-coding regions. *Development* **148**, dev199994 (2021).
582 10.1242/dev.199994.

583 17. Anzalone, A. V. et al. Search-and-replace genome editing without double-strand breaks or
584 donor DNA. *Nature* **576**, 149–157 (2019). 10.1038/s41586-019-1711-4.

585 18. Petri, K. et al. CRISPR prime editing with ribonucleoprotein complexes in zebrafish and
586 primary human cells. *Nat. Biotechnol.* **40**, 189–193 (2022). 10.1038/s41587-021-00901-y.

587 19. Davis, J. R. et al. Efficient prime editing in mouse brain, liver and heart with dual AAVs.
588 *Nat. Biotechnol.* **42**, 253–264 (2024). 10.1038/s41587-023-01758-z.

589 20. Ely, Z. A. et al. A prime editor mouse to model a broad spectrum of somatic mutations in
590 vivo. *Nat. Biotechnol.* **42**, 424–436 (2024). 10.1038/s41587-023-01783-y.

591 21. Adikusuma, F. et al. Optimized nickase- and nuclease-based prime editing in human and
592 mouse cells. *Nucleic Acids Res.* **49**, 10785–10795 (2021). 10.1093/nar/gkab792.

593 22. Peterka, M. et al. Harnessing DSB repair to promote efficient homology-dependent and -
594 independent prime editing. *Nat. Commun.* **13**, 1240 (2022). 10.1038/s41467-022-28771-1.

595 23. Li, X. et al. Development of a versatile nuclease prime editor with upgraded precision. *Nat.*
596 *Commun.* **14**, 305 (2023). 10.1038/s41467-023-35870-0.

597 24. Kortüm, K. M. et al. Targeted sequencing of refractory myeloma reveals a high incidence
598 of mutations in CRBN and Ras pathway genes. *Blood* **128**, 1226–1233 (2016). 10.1182/blood-
599 2016-02-698092.

600 25. Ito, T. et al. Identification of a primary target of thalidomide teratogenicity. *Science* **327**,
601 1345–1350 (2010). 10.1126/science.1177319.

602 26. Donovan, K. A. et al. Thalidomide promotes degradation of SALL4, a transcription factor
603 implicated in Duane Radial Ray syndrome. *eLife* **7**, e38430 (2018). 10.7554/eLife.38430.

604 27. Fink, E. C. et al. CrbnI391V is sufficient to confer in vivo sensitivity to thalidomide and its
605 derivatives in mice. *Blood* **132**, 1535–1544 (2018). 10.1182/blood-2018-05-852798.

606 28. Zhang, W. et al. Enhancing CRISPR prime editing by reducing misfolded pegRNA
607 interactions. *eLife* **12**, RP90948 (2024). 10.7554/eLife.90948.

608 29. Ponnienselvan, K. et al. Reducing the inherent auto-inhibitory interaction within the
609 pegRNA enhances prime editing efficiency. *Nucleic Acids Res.* **51**, 6966–6980 (2023).
610 10.1093/nar/gkad456.

611 30. van Bokhoven, H. et al. Mutation of the gene encoding the ROR2 tyrosine kinase causes
612 autosomal recessive Robinow syndrome. *Nat. Genet.* **25**, 423–426 (2000). 10.1038/78113.

613 31. Afzal, A. R. et al. Recessive Robinow syndrome, allelic to dominant brachydactyly type B,
614 is caused by mutation of ROR2. *Nat. Genet.* **25**, 419–422 (2000). 10.1038/78107.

32. Lima, A. R. et al. Phenotypic and mutational spectrum of ROR2-related Robinow syndrome. *Hum. Mutat.* **43**, 900–918 (2022). 10.1002/humu.24375.

33. Bacino, C. A. ROR2-related Robinow syndrome. *GeneReviews* (2005). University of Washington, Seattle. https://www.ncbi.nlm.nih.gov/books/NBK1240/.

34. Zhang, C., Brunt, L., Ono, Y., Rogers, S. & Scholpp, S. Cytoneme-mediated transport of active Wnt5b-Ror2 complexes in zebrafish. *Nature* **625**, 126–133 (2024). 10.1038/s41586-023-06850-7.

35. Mattes, B. et al. Wnt/PCP controls spreading of Wnt/β-catenin signals by cytonemes in vertebrates. *eLife* **7**, e36953 (2018). 10.7554/eLife.36953.

36. Brunt, L. et al. Vangl2 promotes the formation of long cytonemes to enable distant Wnt/β-catenin signaling. *Nat. Commun.* **12**, 2058 (2021). 10.1038/s41467-021-22393-9.

37. Bai, Y. et al. Ror2 receptor mediates Wnt11 ligand signaling and affects convergence and extension movements in zebrafish. *J. Biol. Chem.* **289**, 20664–20676 (2014). 10.1074/jbc.M114.586099.

38. Dranow, D. B., Le Pabic, P. & Schilling, T. F. The non-canonical Wnt receptor Ror2 is required for cartilage cell polarity and morphogenesis of the craniofacial skeleton in zebrafish. *Development* **150**, dev201273 (2023). 10.1242/dev.201273.

39. Antoniou, P. et al. Modified pegRNAs mitigate scaffold-derived prime editing by-products. *Nat. Commun.* **16**, 3374 (2025). 10.1038/s41467-025-58653-1.

40. Schwabe, G. C. et al. Ror2 knockout mouse as a model for the developmental pathology of autosomal recessive Robinow syndrome. *Dev. Dyn.* **229**, 400–410 (2004). 10.1002/dvdy.10466.

41. Elworthy, S., Hargrave, M., Knight, R., Mebus, K. & Ingham, P. W. Expression of multiple slow myosin heavy chain genes reveals a diversity of zebrafish slow twitch muscle fibres with differing requirements for Hedgehog and Prdm1 activity. *Development* **135**, 2115-2126 (2008). 10.1242/dev.015719.

42. Dang, C. V. & Lee, W. M. Identification of the human c-myc protein nuclear translocation signal. *Mol. Cell. Biol.* **8**, 4048–4054 (1988). 10.1128/mcb.8.10.4048-4054.1988.

43. Hodel, M. R., Corbett, A. H. & Hodel, A. E. Dissection of a nuclear localization signal. *J. Biol. Chem.* **276**, 1317–1325 (2001). 10.1074/jbc.M008522200.

44. Ray, M., Tang, R., Jiang, Z. & Rotello, V. M. Quantitative tracking of protein trafficking to the nucleus using cytosolic protein delivery by nanoparticle-stabilized nanocapsules. *Bioconjug. Chem.* **26**, 1004–1007 (2015). 10.1021/acs.bioconjchem.5b00141.

45. Mosimann, C. et al. Site-directed zebrafish transgenesis into single landing sites with the phiC31 integrase system. *Dev. Dyn.* **242**, 949–963 (2013). 10.1002/dvdy.23989.

46. Roberts, J. A. et al. Targeted transgene integration overcomes variability of position effects in zebrafish. *Development* **141**, 715–724 (2014). 10.1242/dev.100347.

651 47. Lalonde, R. L. et al. pIGLET: Safe harbor landing sites for reproducible and efficient
652 transgenesis in zebrafish. *Sci. Adv.* **10**, eadn6603 (2024). 10.1126/sciadv.adn6603.

653 48. Kuroki-Kami, A. et al. Targeted gene knockin in zebrafish using the 28S rDNA-specific
654 non-LTR-retrotransposon R2Ol. *Mob. DNA* **10**, 23 (2019). 10.1186/s13100-019-0167-2.

655 49. Komor, A. C., Kim, Y. B., Packer, M. S., Zuris, J. A. & Liu, D. R. Programmable editing of
656 a target base in genomic DNA without double-stranded DNA cleavage. *Nature* **533**, 420–424
657 (2016). 10.1038/nature17946.

658 50. Gaudelli, N. M. et al. Programmable base editing of A•T to G•C in genomic DNA without
659 DNA cleavage. *Nature* **551**, 464–471 (2017). 10.1038/nature24644.

660 51. Zhang, Y. et al. Programmable base editing of zebrafish genome using a modified CRISPR-
661 Cas9 system. *Nat. Commun.* **8**, 118 (2017). 10.1038/s41467-017-00175-6.

662 52. Rees, H. A. et al. Improving the DNA specificity and applicability of base editing through
663 protein engineering and protein delivery. *Nat. Commun.* **8**, 15790 (2017).
664 10.1038/ncomms15790.

665 53. Zhao, Y., Shang, D., Ying, R., Cheng, H. & Zhou, R. An optimized base editor with efficient
666 C-to-T base editing in zebrafish. *BMC Biol.* **18**, 190 (2020). 10.1186/s12915-020-00923-z.

667 54. Rosello, M. et al. Precise base editing for the in vivo study of developmental signaling and
668 human pathologies in zebrafish. *eLife* **10**, e65552 (2021). 10.7554/eLife.65552.

669 55. Qin, W. et al. ABE-ultramax for high-efficiency biallelic adenine base editing in zebrafish.
670 *Nat. Commun.* **15**, 5613 (2024). 10.1038/s41467-024-49943-1.

671 56. Zhang, Y. et al. Cytosine base editors with increased PAM and deaminase motif flexibility
672 for gene editing in zebrafish. *Nat. Commun.* **15**, 9526 (2024). 10.1038/s41467-024-53735-y.

673 57. Vanhooydonck, M. et al. Prime editing outperforms homology-directed repair as a tool for
674 CRISPR-mediated variant knock-in in zebrafish. *Lab Anim.* **54**, 165–172 (2025).
675 10.1038/s41684-025-01560-1.

676 58. Kim-Yip, R. P. et al. Efficient prime editing in two-cell mouse embryos using PEmbryo.
677 *Nat. Biotechnol.* **42**, 1822–1830 (2024). 10.1038/s41587-023-02106-x.

678 59. Salem, A. R. et al. Prime editing in mice with an engineered pegRNA. *Vascul. Pharmacol.*
679 **154**, 107269 (2024). 10.1016/j.vph.2023.107269.

680 60. Ben-Shachar, S. et al. Dominant versus recessive traits conveyed by allelic mutations - to
681 what extent is nonsense-mediated decay involved? *Clin. Genet.* **75**, 394–400 (2009).
682 10.1111/j.1399-0004.2008.01114.x.

683 61. Wittkopp, N. et al. Nonsense-mediated mRNA decay effectors are essential for zebrafish
684 embryonic development and survival. *Mol. Cell. Biol.* **29**, 3517–3528 (2009).
685 10.1128/MCB.00177-09.

686 62. Lai, S. et al. Effect of nonsense-mediated mRNA decay factor SMG9 deficiency on
687 premature aging in zebrafish. *Commun. Biol.* **7**, 654 (2024). 10.1038/s42003-024-06356-6.

688 63. Koeppel, J. et al. Prediction of prime editing insertion efficiencies using sequence features
689 and DNA repair determinants. *Nat. Biotechnol.* **41**, 1446–1456 (2023). 10.1038/s41587-023-
690 01678-y.

691 64. Chen, P. J. et al. Enhanced prime editing systems by manipulating cellular determinants of
692 editing outcomes. *Cell* **184**, 5635–5652.e29 (2021). 10.1016/j.cell.2021.09.018.

693 65. Ferreira da Silva, J. et al. Prime editing efficiency and fidelity are enhanced in the absence
694 of mismatch repair. *Nat. Commun.* **13**, 760 (2022). 10.1038/s41467-022-28442-1.

695 66. Nelson, J. W. et al. Engineered pegRNAs improve prime editing efficiency. *Nat. Biotechnol.*
696 **40**, 402–410 (2022). 10.1038/s41587-021-01039-7.

697 67. Yan, J. et al. Improving prime editing with an endogenous small RNA-binding protein.
698 *Nature* **628**, 639–647 (2024). 10.1038/s41586-024-07259-6.

699 68. Basharat, R., Rizzo, G., Zoodsma, J. D., Wollmuth, L. P. & Sirotkin, H. I. Optimizing prime
700 editing in zebrafish. *CRISPR J.* **8**, 426–435 (2025). 10.1177/25731599251380500.

701 69. Qin, L. & Lin, Q. Optimized ribonucleoprotein complexes enhance prime editing efficiency
702 in zebrafish. *Animals* **15**, 2295 (2025). 10.3390/ani15152295.

703 70. Kosicki, M., Tomberg, K. & Bradley, A. Repair of double-strand breaks induced by
704 CRISPR-Cas9 leads to large deletions and complex rearrangements. *Nat. Biotechnol.* **36**, 765–
705 771 (2018). 10.1038/nbt.4192.

706 71. Adikusuma, F. et al. Large deletions induced by Cas9 cleavage. *Nature* **560**, E8–E9 (2018).
707 10.1038/s41586-018-0380-z.

708 72. Leibowitz, M. L. et al. Chromothripsis as an on-target consequence of CRISPR-Cas9
709 genome editing. *Nat. Genet.* **53**, 895–905 (2021). 10.1038/s41588-021-00838-7.

710 73. Paull, G. C. et al. Variability in measures of reproductive success in laboratory-kept
711 colonies of zebrafish and implications for studies addressing population-level effects of
712 environmental chemicals. *Aquat. Toxicol.* **87**, 115–126 (2008). 10.1016/j.aquatox.2008.01.008.

713 74. Meeker, N. D., Hutchinson, S. A., Ho, L. & Trede, N. S. Method for isolation of PCR-ready
714 genomic DNA from zebrafish tissues. *Biotechniques* **43**, 610–614 (2007). 10.2144/000112619.

715 75. Clement, K. et al. CRISPResso2 provides accurate and rapid genome editing sequence
716 analysis. *Nat. Biotechnol.* **37**, 224–226 (2019). 10.1038/s41587-019-0032-3

717 **Figures**

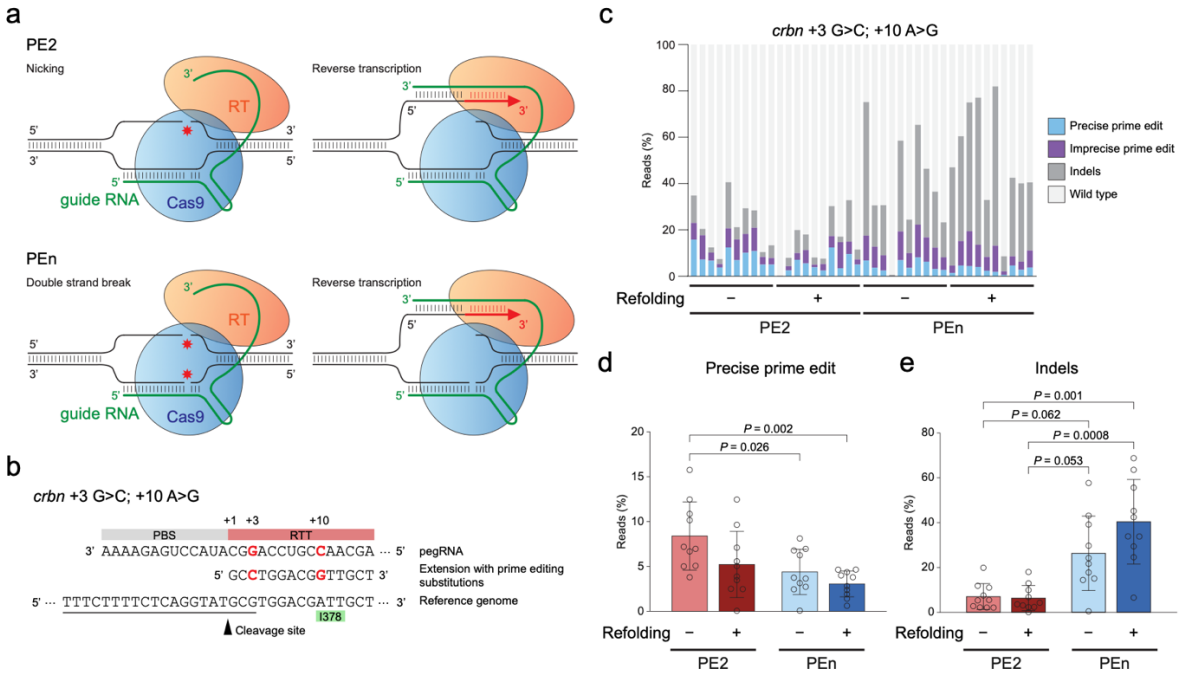

718

719 **Fig. 1 Prime editing substitution in the zebrafish *crbn* gene, comparing Cas9-nickase-**
720 **based and nuclease-based Prime Editors.** a, Schematic illustration of the functioning of
721 prime editing by the Cas9-nickase-based Prime Editor (PE2) and the nuclease-based Prime
722 Editor (PEn). b, Schematic illustration of the strategy for prime editing substitution in *crbn*
723 gene. The nucleotides for substitution are indicated in red. The guide RNA (gRNA) target
724 sequence is underlined. c–e, Comparison between PEn and PE2 in prime editing substitution
725 in the *crbn* gene with the pegRNA refolding procedure. Proportions of editing outcomes in
726 individual injected embryos are shown by amplicon sequencing (c), alongside quantitative
727 analyses of precise prime edits (d) and indels (e) comparing experimental conditions (n = 10
728 per group). P-values were determined using one-way ANOVA with Tukey's multiple
729 comparison test in (d), and the Kruskal-Wallis test with Dunn's multiple comparison test in (e).
730 Error bars in the bar graphs represent the mean and standard deviation, and individual data
731 points indicate values from single injected embryos.

732

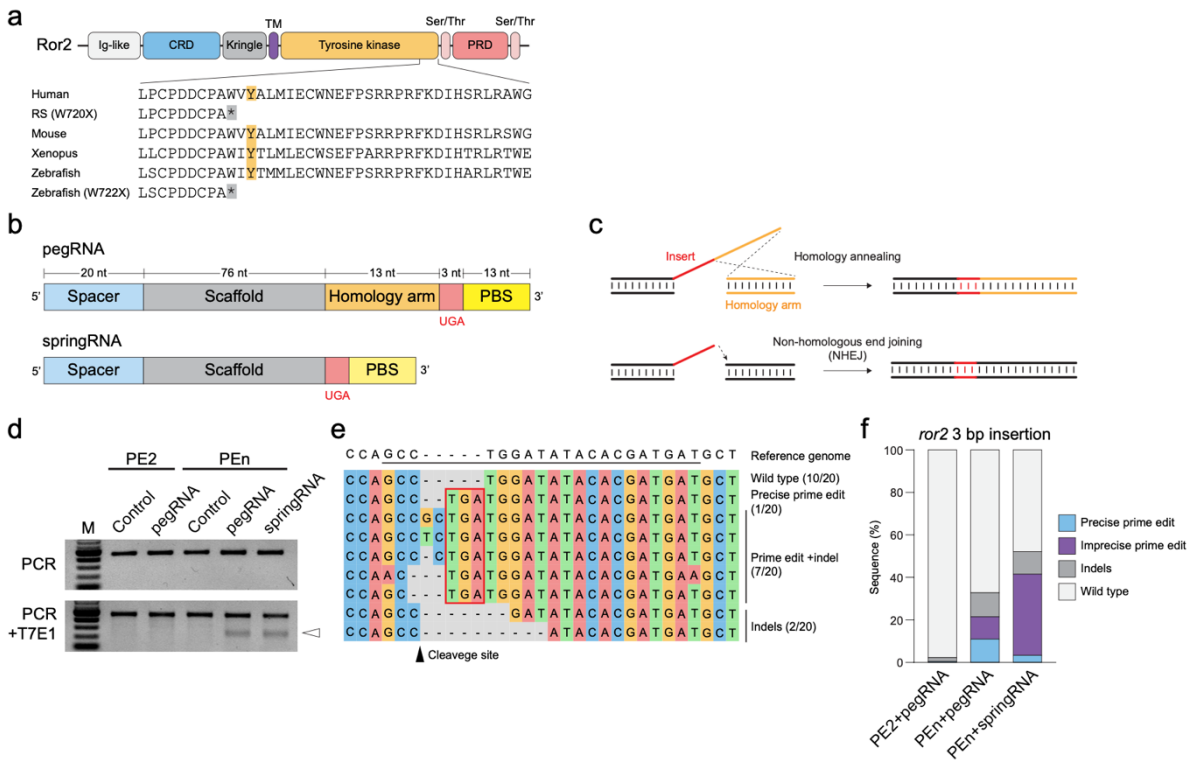

Fig. 2 Prime editing insertion in zebrafish *ror2* gene using Cas9-nuclease-based Prime Editor. a, Schematic illustration of the functional domains in the Ror2 protein and alignment of partial amino acid sequences within the tyrosine kinase domain. Sequences from multiple species, including those related to Robinow syndrome (RS) in humans W720X and the corresponding zebrafish W722X mutant, are aligned. The conserved tyrosine residue is highlighted. b, Schematic illustration of guide RNA (gRNA) designs for prime editing insertion in *ror2*. c, Schematic illustration of prime editing insertion by Cas9-nuclease-based Prime Editor (PEn). An additional DNA fragment, reverse-transcribed at the target cleavage site, containing the programmed insertion, is integrated into the genome via homology-directed repair or non-homologous end joining. d, Agarose gel images of genomic PCR products from embryos injected with Prime Editor mRNA and pegRNA/springRNA. PCR products of the *ror2* target region (top) and those after digestion with T7 endonuclease I (T7E1, bottom). e, Sequence alignment of the edits in the *ror2* target site obtained from embryos injected with PEn/springRNA. Prime editing insertion (TGA) is outlined, and the gRNA target sequence is underlined. f, Quantitative comparison of editing outcomes using different combinations of Prime Editor and gRNA. The proportion of sequence reads with each type of edit in amplicon sequencing is presented.

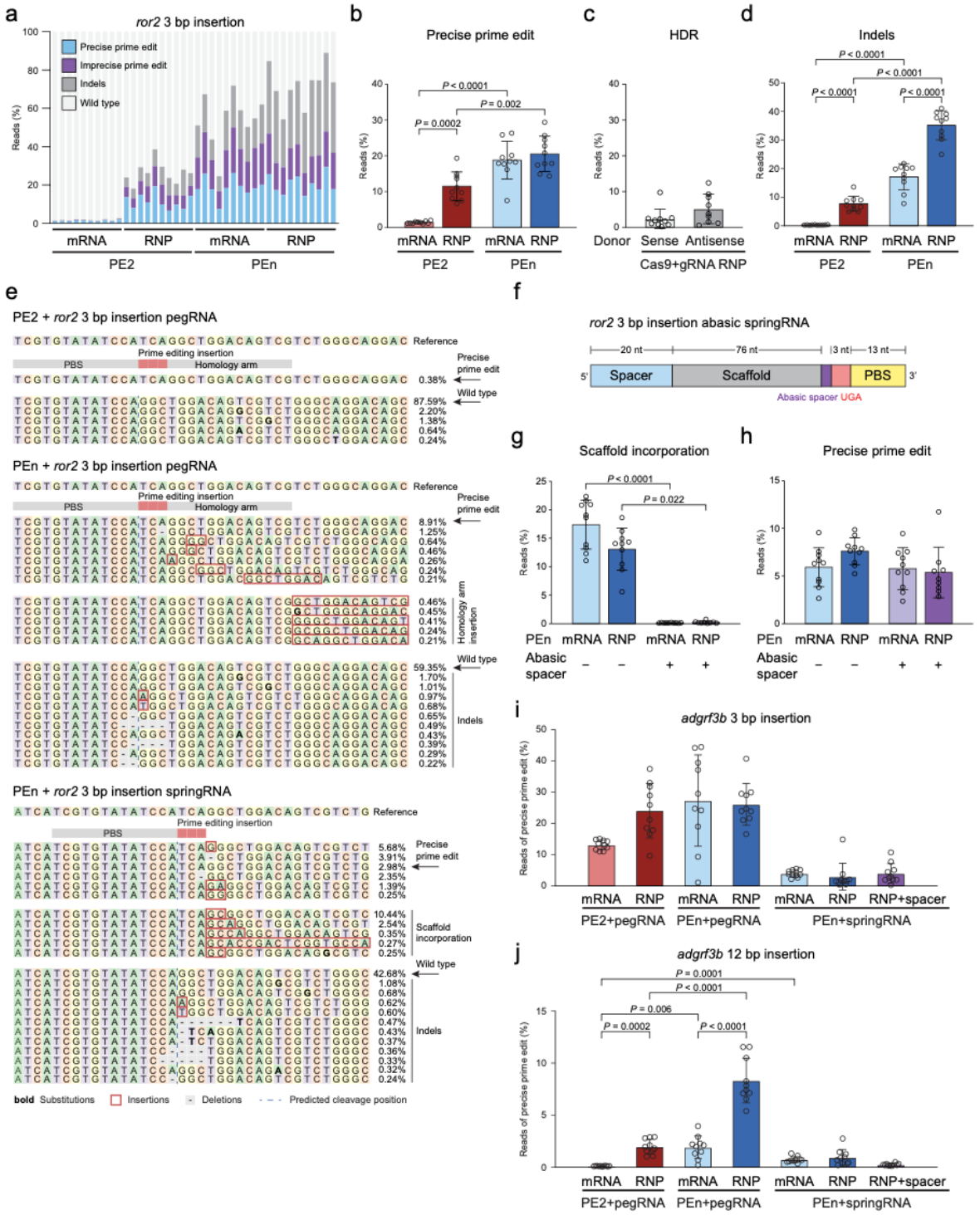

752

753 **Fig. 3 Comparing different prime editing approaches in zebrafish embryos.** a and b,
754 Comparison between PEn and PE2 in prime editing insertion into *ror2* with various delivery
755 methods. The proportion of editing outcomes in individual injected embryos was assessed
756 through amplicon sequencing (a), along with a quantitative analysis of precise prime edit (b)
757 and indels (d) across experimental conditions (n = 10 per group). c, Proportion of reads with
758 precise HDR-mediated insertion in *ror2* using single-stranded sense or antisense donor DNAs

759 with 40 bp homology arms. d, Proportion of reads with indels comparing PEn and PE2 in prime
760 editing insertion into *ror2*. e, Sequence alignment of edits in prime editing insertion in *ror2* via
761 PE2 mRNA/pegRNA (top), PEn mRNA/pegRNA (middle), and PEn mRNA/springRNA
762 (bottom) combinations. f, Schematic illustration of springRNA design featuring an abasic RNA
763 spacer for prime editing insertion in *ror2*. g and h, Proportion of reads with scaffold
764 incorporation (g) and precise prime edit (h) as determined by amplicon sequencing of prime
765 editing insertion in *ror2* using control and abasic springRNA (n = 10 per group; one sample of
766 the PEn RNP/abasic springRNA combination was excluded from analysis due to low read
767 count). i and j, Prime editing insertion in the *adgrf3b* gene using PE2 and PEn. The proportion
768 of reads with a precise 3 bp (i) and 12 bp insertion (j) was evaluated (n = 10 per group). P-
769 values were determined by Welch's one-way ANOVA with Dunnett T3 multiple comparison
770 test in b, d, and j, and Kruskal-Wallis test with Dunn's multiple comparison test in g. Error bars
771 in bar graphs represent the mean and standard deviation, and each individual data point
772 indicates the value from a single injected embryo.

773

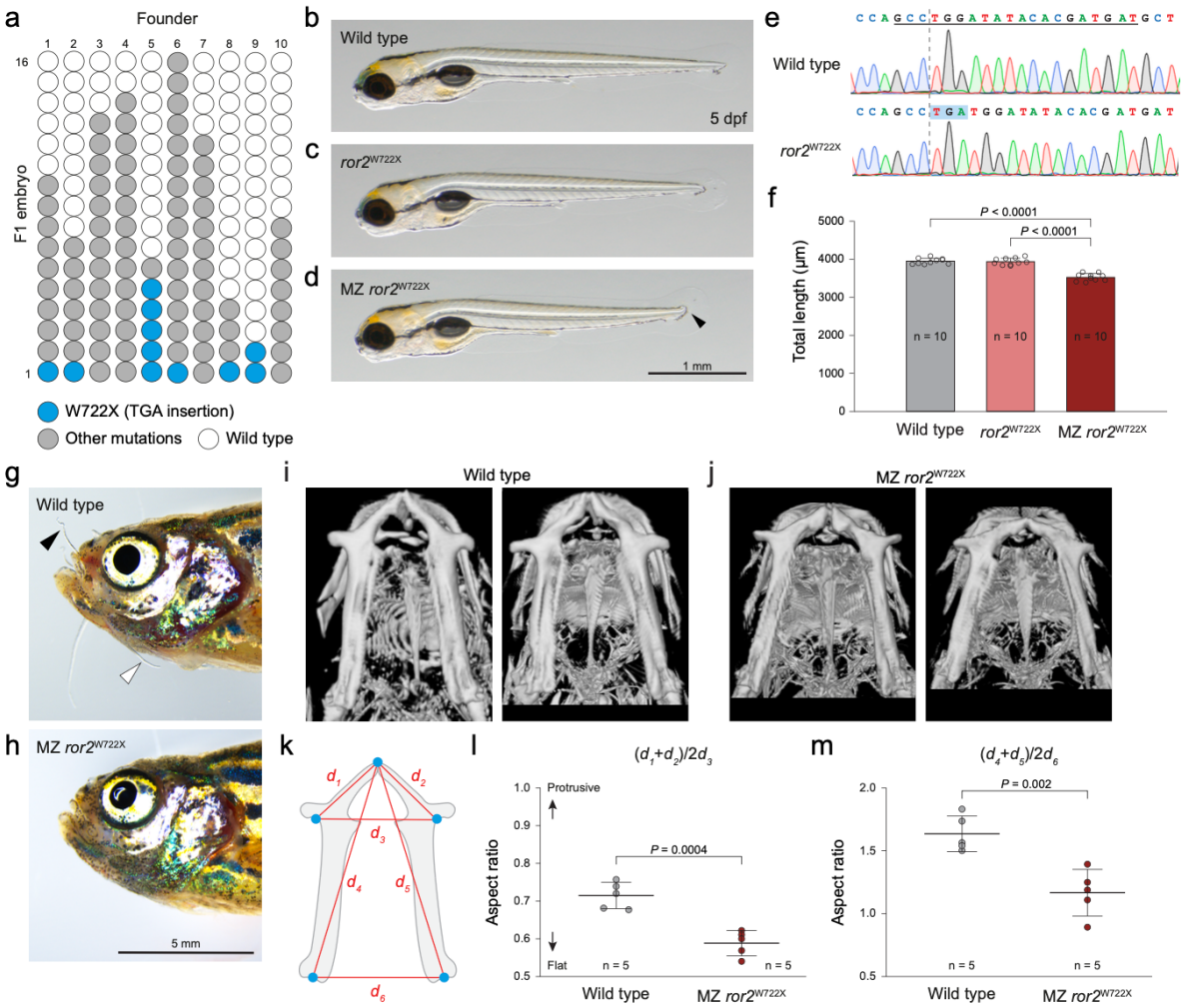

774

775 **Fig. 4 Generation and characterisation of stable *ror2*^{W722X} mutant.** a, Summary of the
776 screening of F1 embryos. Sixteen embryos were genotyped per F0 founder. Each circle
777 represents the genotype of a single embryo. The embryos were obtained by outcrossing the
778 injected founder with wild-type fish; thus, all embryos with the mutation are heterozygous. b-
779 d, Lateral images of wild type (b), zygotic *ror2*^{W722X} mutant (c), and maternal-zygotic (MZ)
780 *ror2*^{W722X} mutant (d) larvae at 5 days post-fertilisation (dpf). e, Sanger sequencing
781 chromatogram of wild type (top) and *ror2*^{W722X} mutant (bottom) at the prime editing target site
782 in *ror2*. Prime editing insertion (TGA) is highlighted. The target sequence of the guide RNA
783 is underlined, and the cleavage site of Cas9 is indicated by a dotted line. f, Quantitative analysis
784 of total length comparing wild type, zygotic *ror2*^{W722X} mutant, and MZ *ror2*^{W722X} mutant at 5
785 dpf. Each data point on the graph represents the value from a single larva (n = 10 per group).
786 P-values were determined by one-way ANOVA with a Tukey multiple comparisons test. Error
787 bars represent the mean and standard deviation. g and h, Lateral images of 1 year old wild type
788 (g) and MZ *ror2*^{W722X} mutant (h). Nasal and maxillary barbels are indicated by black and white

789 arrowheads, respectively. i and j, Reconstructed computed tomography images of
790 cranioskeletal morphologies in 1 year old wild type (i) and MZ *ror2*^{W722X} mutant (j). The
791 images are ventral view and anterior is to the top. k, Schematic illustration of mandibular bone
792 from the ventral view and the location of geographical points for annotation to measure linear
793 distances and calculate the aspect ratios. l and m, Quantitative analysis of the aspect ratios in
794 the mandible comparing wild type and MZ *ror2*^{W722X} mutant. Aspect ratio of anterior part (l)
795 and whole structure (m) of the mandible was analysed. The p-values were determined using
796 unpaired t-test. Error bars represent the mean and standard deviation, while individual data
797 points on the graph indicate values from single reconstructed image.

798

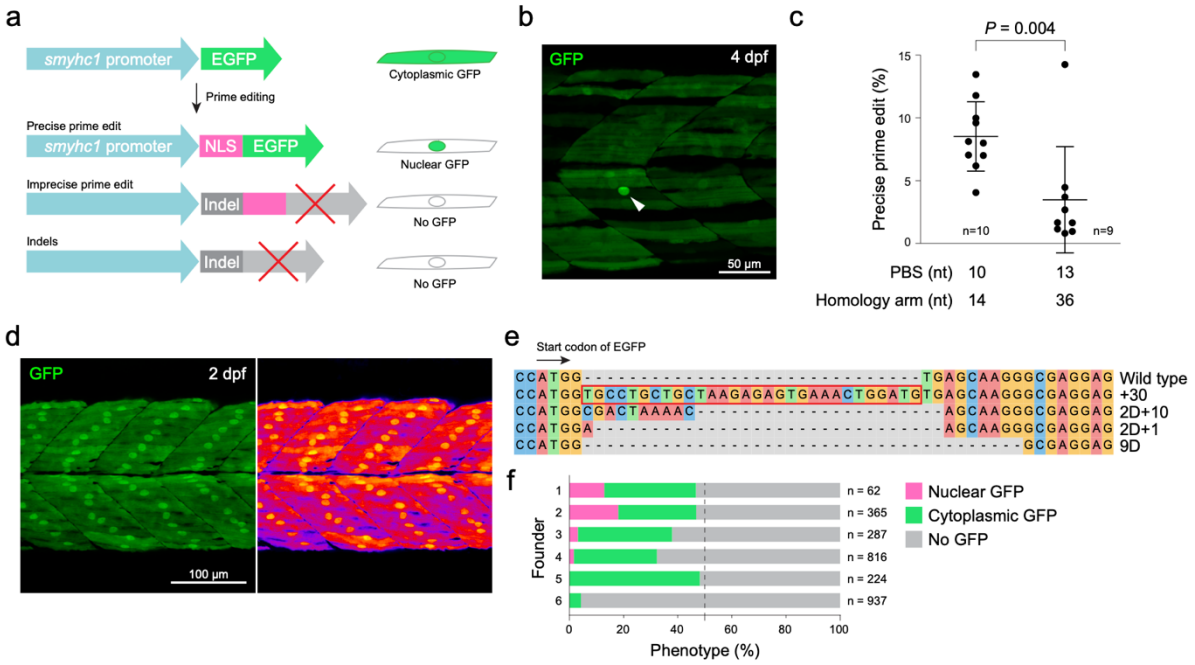

799

800 **Fig. 5 Prime editing to insert a nuclear localisation signal sequence into the *smyhc1:gfp***
801 **transgene.** a, Schematic representation of the prime editing insertion of the nuclear localisation
802 signal (NLS) sequence into the *smyhc1:gfp* transgene and the expected eGFP expression in
803 slow-twitch muscle fibres. b, Confocal microscopy image of the trunk muscle in *smyhc1:gfp*
804 larvae at 4 days post-fertilisation (dpf) that were injected with the PEn RNP complex for the
805 prime editing NLS insertion. Putative nuclear GFP expression is indicated by an arrowhead.
806 Anterior is positioned to the left. c, Quantitative analysis of the efficiency of precise NLS
807 insertion via amplicon sequencing. Two pegRNAs of differing lengths are compared (n = 10
808 per group, with one sample excluded from the analysis due to low read count). The p-value
809 was determined using the Mann-Whitney U test. Error bars represent the mean and standard

deviation, while individual data points on the graph indicate values from single injected larvae. d, Confocal microscopy images of the trunk muscle of F1 larvae exhibiting nuclear GFP expression at 2 dpf, obtained from founder 1 (see panel f). The GFP fluorescence channel (left) and pseudo-colour (right) images are shown. Anterior is to the left. e, Sequence alignment of the edits in the target site obtained from F1 embryos exhibiting nuclear GFP expression (founder 1). The NLS sequence is outlined in red. f, Summary of F1 embryo screening. F1 embryos obtained from 6 founders are categorised based on the GFP expression pattern. The embryos were produced by outcrossing the heterozygous *smyhc1:gfp* founder injected with the PEn RNP complex to wild type; thus, half of the embryos are expected to be negative for the *smyhc1:gfp* transgene.